Research in Astron. Astrophys. Vol.0 (200x) No.0, 000–000
http://www.raa-journal.org *http://www.iop.org/journals/raa*

***R**esearch in*
***A**stronomy and*
***A**strophysics*

arXiv:1603.02404v1 [astro-ph.HE] 8 Mar 2016

UV and X-Ray Variability of the Narrow-Line Seyfert 1 Galaxy Ark 564

Savithri H. Ezhikode[1], Gulab C. Dewangan[2], Ranjeev Misra[2], Shruti Tripathi[3], Ninan Sajeeth Philip[1] and Ajit K. Kembhavi[2]

[1] Department of Physics, St. Thomas College, Kozhencherry, Kerala, India
[2] Inter-University Centre for Astronomy & Astrophysics, Post Bag 4, Ganeshkhind, Pune, India
[3] Physics Department, Bishops University, 2600 College Street, Sherbrooke, QC, Canada J1M 1Z7

Abstract We analyse eight *XMM-Newton* observations of the bright Narrow-Line Seyfert 1 galaxy Arakelian 564 (Ark 564). These observations, separated by ~ 6 days, allow us to look for correlations between the simultaneous UV emission (from the Optical Monitor) with not only the X-ray flux but also with the different X-ray spectral parameters. The X-ray spectra from all the observations are found to be adequately fitted by a double Comptonization model where the soft excess and the hard X-ray power law are represented by thermal Comptonization in a low temperature plasma and hot corona, respectively. Apart from the fluxes of each component, the hard X-ray power law index is found to be variable. These results suggest that the variability is associated with changes in the geometry of the inner region. The UV emission is found to be variable and well correlated with the high energy index while the correlations with the fluxes of each component are found to be weaker. Using viscous time-scale arguments we rule out the possibility that the UV variation is due to fluctuating accretion rate in the outer disc. If the UV variation is driven by X-ray reprocessing, then our results indicate that the strength of the X-ray reprocessing depends more on the geometry of the X-ray producing inner region rather than on the X-ray luminosity alone.

Key words: galaxies: active — galaxies: Seyfert — galaxies: individual (Ark 564) — X-rays: galaxies

1 INTRODUCTION

Active Galactic Nuclei (AGN) emit over a wide range of the electromagnetic spectrum and their spectra show strong optical/UV emission lines which are not present in the spectrum of a normal galaxy. AGN are believed to harbour a supermassive black hole (SMBH) of mass $\sim 10^6 - 10^9 M_\odot$. The accretion of matter on to the SMBH is the major source of radiation in AGN, and they can outshine the stellar emission of the host galaxy (e.g. Peterson 1997; Beckmann & Shrader 2012). According to the standard model of AGN, the matter accreted from the host galaxy forms an accretion disc surrounding the central black hole and the spectrum emitted from the disc peaks in the optical/UV band. Furthermore, there is a hot corona above the disc which inverse Compton scatters the disc photons resulting in X-ray emission. The broadband X-ray emission is one of the fundamental characteristics defining AGN (e.g. Beckmann & Shrader (2012)).

A significant property of AGN is their continuum variability over the entire electromagnetic spectrum. AGN, in general, show strong X-ray variability and a subset of AGN called Narrow Line Seyfert 1 (NLS1) shows extreme variability (e.g. Boller et al. (1996)). Relationship between emission in different

bands provides important insights into the nature of AGN. A number of previous studies have shown that X-ray and optical/UV variations in AGN are well correlated (Nandra et al., 1998; Edelson et al., 1996; Smith & Vaughan, 2007; McHardy et al., 2014). There are two basic models to explain the UV variability in AGN: the UV variability could be due to accretion rate variation in the outer disc or it could be due to X-ray reprocessing (e.g. McHardy et al. (2014)). In the first case, the UV flux variation can provide information about accretion rate variation while in the second case, the correlation between the soft/hard X-ray component and the UV emission can reveal which X-ray spectral component has the greater affect on the outer disc.

A multiwavelength campaign undertaken by Edelson et al. (1996) observed a strong correlation between the X-ray, UV and optical variability in the Seyfert 1 (Sy 1) galaxy NGC 4151, with no detectable lags. The UV observations were taken with a sampling interval of $\sim$0.05 d while the X-ray observations were taken twice per day. The obtained results suggest that UV emission in the source is produced by the reprocessing of primary X-rays. A recent study by McHardy et al. (2014) investigates the relationship between the X-ray, UV and optical variability of the Sy 1 galaxy NGC 5548. They analysed 554 *Swift* (XRT $\&$ UVOT) observations of the source, typically taken every two days, over a period of 750 d. The study strengthens the short time-scale correlations between X-ray and UV/optical bands and the lag measurements of this object also lead to the conclusion that UV/optical variability is due to the reprocessing of X-rays. Shemmer et al. (2003) studied the X-ray$-$optical correlation of the NLS1 galaxy NGC 4051 based on the data available from 2000 May-July observations. The optical data were retrieved from *Wise Observatory* and X-ray data from *RXTE*. They obtained *RXTE* data from 251 observations with an interval of 6 h. They conclude that the observed X-ray$-$optical correlation in the source can be explained as a combined effect of X-ray reprocessing and the propagation of perturbations from the outer disc to the X-ray emitting region.

In this work, we study the source Arakelian 564 (Ark 564) which is an X-ray bright NLS 1 (Brandt et al., 1994; Vaughan et al., 1999) found in the nearby universe with redshift z = 0.0247. It is a well studied source which is known to accrete at super-Eddington rate (Mullaney et al., 2009). Earlier studies have shown that the high energy spectrum of Ark 564 is characterised by a steep power law (Vignali et al., 2004; Matsumoto et al., 2004). Vignali et al. (2004) detected absorption corresponding to the O VII K-edge ($\sim$ 0.73 keV) in two different *XMM-Newton* observations (2000 & 2001) of the source. They also obtained evidence for significant X-ray variability of the object both at low and high energies. The spectral variability analysis of Ark 564 was carried out by Brinkmann et al. (2007) with the longest exposure observation available from *XMM-Newton*. They found that both the soft and hard X-ray flux are highly variable on short time-scales. The cross-correlation analysis of light curves showed some delay in the observation of hard band photons with respect to soft band photons. The high energy photon index Γ was also variable and it was found to be leading the variations in soft and hard energy bands. A previous study using ASCA observations by Bian & Zhao (2003) determined the relations between hard X-ray variability, photon index Γ and Eddington ratio $\dot{m}$ of a sample of AGN, including Ark 564. They found that the X-ray variability and central black hole mass M_{BH} are strongly anti-correlated while a weak correlation exists for the variability and $\dot{m}$. This means that small value of M_{BH} is responsible for the variability of NLS1s. The study also discovered a strong correlation between Γ and $\dot{m}$.

Smith & Vaughan (2007) examined the X-ray and optical variability of Ark 564 and seven other Sy 1 galaxies over a period of $\sim$1 d. The source was variable in X-rays, but not in the optical band. But another study by Shemmer et al. (2001) investigated the optical$-$UV$-$X-ray connection of Ark 564 over a longer period of time of $\sim$50 d. It was a two year long multiwavelength monitoring program in which the X-ray observations were covered with *RXTE* and *ASCA* while the UV observations with *HST*. They observed a significant correlation of the continua, where the X-ray continuum was followed by UV with a time lag of 0.4 d which in turn was followed by the optical band by $\sim$2 d. The soft X-ray flux was also found to be well correlated with the hard band flux with zero time lag. Rapid X-ray variations of $\lesssim$1 d was observed in the source, but the mean flux was constant on time-scales $>$30 d.

A study has been carried out by Dewangan et al. (2007) of the soft excess emission from the NLS1 galaxies Ark 564 and Mrk 1044. They argued that the soft excess emission from Ark 564 can be ex-

plained by considering a two-component corona in the source. According to their model, the geometry of the corona is such that it consists two different physical regions, one being optically thick and cool while the other a high-temperature, optically thin region. The hot corona extends above the low-temperature corona while the latter is coupled to the inner part of the accretion disc. The optical/UV photons emitted from the accretion disc are Comptonized by the optically thick corona leading to the soft X-ray emission. The geometry suggests that a fraction of these scattered photons again get inverse Compton scattered by the optically thin corona giving rise to the hard X-ray spectrum.

In this work, we examine the correlation between the X-ray and UV emission from Ark 564, by using eight *XMM-Newton* observations in 2011. The data from these observations have already been analysed to study the observed time lag between the soft and hard X-ray emissions (Legg et al., 2012) and the frequency-dependent Fe K lags (Kara et al., 2013). Legg et al. (2012) detected a delayed ($\sim 1000s$) hard X-ray emission in the $4-7.5$ keV with respect to a flaring in the soft X-ray band ($0.4-1$ keV). In view of these results Giustini et al. (2015) reported on the X-ray spectral properties using *XMM-Newton* and *Suzaku* observations of Ark 564 by analysing the time-averaged, flux-selected and time-resolved spectra. They interpreted the delayed hard excess component as the reprocessing of soft photon flares Compton up-scattered in a medium situated at $10-100$ of gravitational radii. However these studies have been limited to the variations in the X-ray band only. Moreover, most of the previous UV/X-ray correlation studies of the source have concentrated on the variation of total X-ray counts or flux with that of the UV band. The high quality X-ray spectral data available by *XMM-Newton* provide us the opportunity to study the variation of different X-ray spectral components with the UV flux. In the present work, we fit the spectra utilising some physical models to obtain the spectral parameters and then study the correlation between these parameters and the UV flux.

The paper is organized as follows. In Section 2, we describe the observations and data reduction. We discuss the variability of the source and spectral analysis in Section 3 and Section 4, respectively. Then we present the correlations in Section 5. Finally, we summarize and discuss our results in Section 6.

2 OBSERVATIONS AND DATA REDUCTION

We used eight observations of Ark 564 taken by *XMM-Newton* between May and July 2011. The details of these pointed observations are given in Table 1. *XMM-Newton* has simultaneous X-ray and UV exposures for all these observations. X-ray data from the European Photon Imaging Camera (EPIC) pn and MOS and UV data from the Optical Monitor (OM) were retrieved from the HEASARC archive. The EPIC-pn camera (Strüder et al., 2001) is positioned such that the incoming radiation from the source enters the primary focus unobstructed, but the EPIC-MOS cameras (Turner et al., 2001) can receive only half of the radiation. The EPIC-pn has large effective area at high energies as well as high quantum efficiency. The pn CCDs are also less susceptible to pile-up during the observations of bright sources. We therefore focus our analysis on the pn data, where the camera was operated in small window mode using a thin filter. OM observations were performed with the *UVW2* filter in the imaging mode. The data reduction is done with SAS version 14.0 using the updated calibration files available in July 2015.

The event lists for EPIC-pn are filtered for single and double (PATTERN=4) best quality (FLAG=0) events in the energy range $0.2-10$ keV. To examine the flaring particle background, light-curves are extracted in the $10-12$ keV band for single events. The intervals of flaring background are then removed from the event list using the threshold rate of 0.1 counts/s obtained from the light curve. The source spectra were extracted from circular regions of radius $36''$around the centre of the source. The background spectra were also extracted from two circular regions of $30''$radii on the same chip, but devoid of source photons. We checked whether any of the observations were affected by pile-up using the SAS task *epatplot*. But no significant deviation in the pattern distribution was observed in any of them. Then we rebinned the data with the tool *specgroup*. While binning we ensured that each bin has a minimum number of 20 counts. Also the oversampling factor was set to 5 such that there are no more than 5 bins to cover the energy resolution.

Table 1 List of *XMM-Newton* Observations of Ark 564.

Observation Number	Observation ID	Start Date	Duration s	PN Exposure Time[1] s	Number of OM Exposures
1	0670130201	2011 May 24	59520	41180	39
2	0670130301	2011 May 30	55919	36510	40
3	0670130401	2011 June 05	63582	31250	45
4	0670130501	2011 June 11	67312	43850	45
5	0670130601	2011 June 17	60919	35570	45
6	0670130701	2011 June 25	64439	29470	43
7	0670130801	2011 June 29	58216	40500	40
8	0670130901	2011 July 01	55915	38400	40

[1]Net exposure time for the EPIC-pn camera

Table 2 X-ray count rate from EPIC-pn in the 0.3−10 keV band (Column 2), UV count rate from OM *UVW2* filter (Column 3) and the corresponding UV flux (Column 4)

Observation Number	EPIC-pn Count Rate counts s^{-1}	UVW2 Count Rate counts s^{-1}	F_{UV} 10^{-15} erg cm^{-2} s^{-1} $Å^{-1}$
1	55.37 ±0.04	1.29 ±0.01	7.39 ±0.04
2	36.33 ±0.03	1.31 ±0.01	7.49 ±0.04
3	37.11 ±0.03	1.22 ±0.01	6.99 ±0.04
4	43.52 ±0.03	1.29 ±0.01	7.37 ±0.04
5	39.78 ±0.03	1.25 ±0.01	7.13 ±0.04
6	24.20 ±0.03	1.18 ±0.01	6.71 ±0.04
7	38.28 ±0.03	1.28 ±0.01	7.30 ±0.04
8	50.91 ±0.04	1.33 ±0.01	7.57 ±0.04

All the Optical Monitor observations were made with *UVW2* filter in the Imaging mode. The SAS task 'omichain' is used to reprocess the OM data, which automatically produces the combined source list of all the filters. But there is a chance that the detection algorithm ('omdetect') may misidentify the source as an extended one, yielding incorrect values of count rate. In order to avoid this, omichain is run with the option 'omdetectdetectextended=no' for the detection and photometry to be performed as on a point source. Then the count rate of the source is obtained form the combined source list of each observation.

3 UV − X-RAY VARIABILITY

We calculated the UV flux F_{UV} of the source from each observation by multiplying the count rate, obtained from the combined source list, with the conversion factor $5.71\times\ 10^{-15}$ erg cm^{-2} s^{-1} $Å^{-1}$ for the *UVW2* filter[1]. Both EPIC-pn and *UVW2* count rates and *UVW2* flux values are given in Table 2. We checked the variability of the source by χ^2 analysis, which measures the deviation of the data points from the best-fit constant. The analysis yielded large χ^2 values for F_{UV} and pn count rate (0.3−10 keV), proving that the source is highly variable in X-ray and UV bands. This is clear from Fig. 1 and Fig. 2.

In order to confirm that the observed variability is not an artifact of the instrument we checked the variability in F_{UV} of other sources which happened to be in the same field of view of all *UVW2* observations. Among these 23 sources five were found to be varying in flux while other sources didn't

[1] See *XMM-Newton* Optical and UV Monitor (OM) Calibration Status document, Talavera 2011 (`http://xmm2.esac.esa.int/docs/documents/CAL-TN-0019.pdf`)

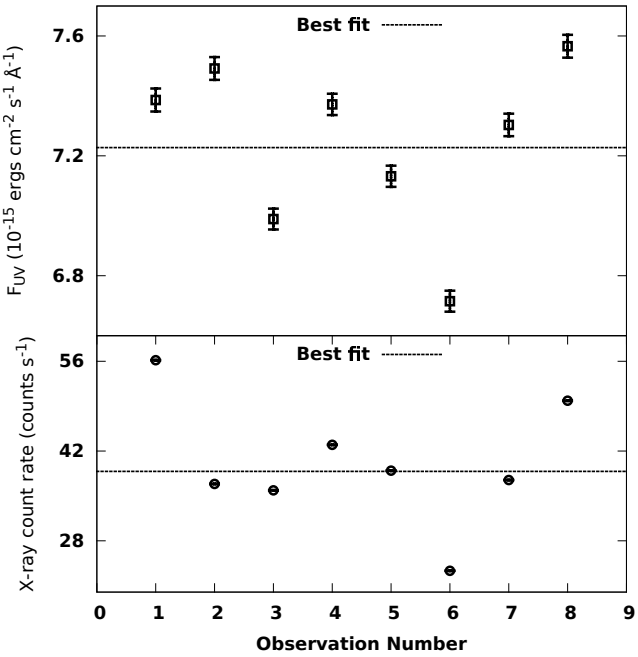

Figure 1 The variation in UV flux F_{UV} obtained from *UVW2* filter of Optical Monitor (Upper panel) and X-ray count rate from EPIC-pn in the range 0.3−10 keV (Lower panel). The horizontal dot-dashed line in each panel corresponds to the constant best-fit value obtained using χ^2 analysis.The vertical error-bars correspond to 1σ errors and in case of the X-ray count rate these are very small.

show any sign of variability. Some of the non-variable sources observed in the same field of view are NVSS J224244+293856, NVSS J224252+294533, 2MASX J22425351+2943125 etc.

We have also calculated the fractional rms variability amplitude of both F_{UV} and pn count rate of Ark 564 and the respective values are ∼0.039 and ∼0.245. This shows that the observed variance in X-ray count rate is large compared to the UV flux variance.

4 SPECTRAL ANALYSIS

The spectral analysis of EPIC-pn and *UVW2* data was done with the XSPEC package (Version 12.8.2). The χ^2 statistic was applied for the spectral fitting and the errors calculated for each parameter correspond to the 90% confidence range, unless otherwise stated.

The template spectral file and response files for the OM data were obtained from the *XMM-Newton* website[2]. We used the template file and the measured count rate to create the spectral file for the analysis of *UVW2* data.

As an example of how we have systematically done the spectral analysis we report here the analysis of Observation Number 2 (Observation ID: 0670130301). The same analysis scheme was applied to the other observations. We started the spectral analysis by fitting the EPIC-pn data, in the energy range 3 to 10 keV, using *powerlaw* together with *TBabs*, the Tuebingen-Boulder ISM absorption model (Wilms et al., 2000). This model with photon index $\Gamma \sim 2.3 - 2.5$ and the Galactic column density

[2] `http://xmm2.esac.esa.int/external/xmm_sw_cal/calib/om_files.shtml`

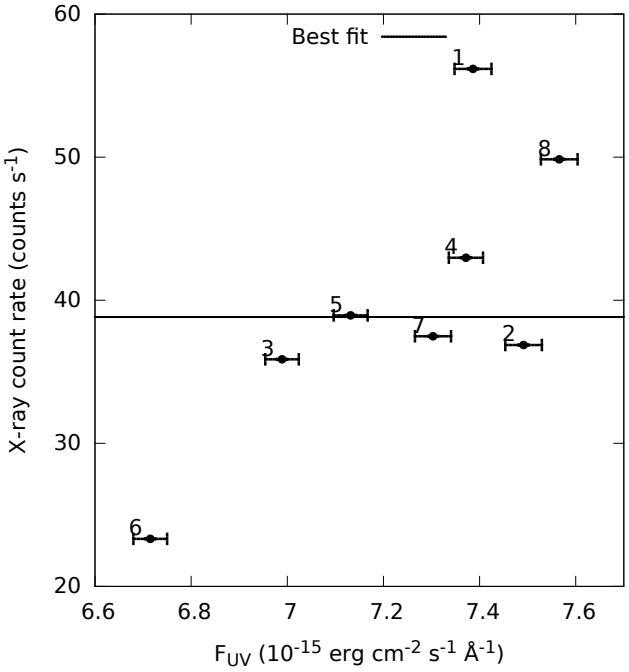

Figure 2 The variation in X-ray count rate from EPIC-pn in the range $0.3-10$ keV. Here, the vertical error-bars (1σ) are very small. The horizontal solid line corresponds to the constant best-fit value obtained using χ^2 analysis.

N_H fixed to $5.41 \times 10^{20} cm^{-2}$ (Kalberla et al., 2005) provides a reasonable fit for all observations. It gave a χ^2 of 239.66 for 162 degrees of freedom (dof) for the second observation. Some excess emission features were detected in the range $6.4-7$ keV which might be attributed to the fluorescent Fe emission line. An improvement in fit, $\Delta\chi^2 = -24.29$, was observed in the second observation, when a red-shifted Gaussian profile (*zgauss*) at $\sim$ 6.6 keV was included. The line appeared to be broad having a width, σ=$0.25^{+0.61}_{-0.11}$ keV. But this broad Gaussian did not fit properly the spectrum of any of the other observations. When we fixed σ of the line to 0.5 keV, all observations could achieve a good fit statistic.

Table 3 Best-fit parameters for the model *uvred*×*zedge*×*zedge*×*TBabs*(*ezdiskbb*+*Simpl*⊗*Nthcomp*+*zgauss*) fitted to the *UVW2* and EPIC-pn spectral data

Model		Observation Number							
Component	Parameter	1	2	3	4	5	6	7	8
zedge 1	E_{edge} (keV)	0.72 ± 0.01	0.69 ± 0.01	0.71 ± 0.01	0.71 ± 0.01	0.71 ± 0.01	0.7 ± 0.01	0.71 ± 0.01	0.71 ± 0.01
	$\tau^{(1)}_{max}$	0.11 ± 0.01	$0.12^{+0.01}_{-0.02}$	0.12 ± 0.02	0.15 ± 0.02	0.11 ± 0.02	0.18 ± 0.03	0.15 ± 0.02	0.12 ± 0.02
zedge 2	E_{edge} (keV)	0.5 ± 0.01	0.51 ± 0.02	0.53 ± 0.02	0.54 ± 0.01	0.52 ± 0.01	$0.54^{+0.01}_{-0.02}$	$0.536^{+0.008}_{-0.003}$	0.52 ± 0.01
	$\tau^{(1)}_{max}$	0.1 ± 0.02	0.05 ± 0.02	0.05 ± 0.03	$0.09^{+0.03}_{-0.02}$	$0.07^{+0.03}_{-0.02}$	0.11 ± 0.04	0.12 ± 0.03	0.06 ± 0.02
Simpl	Γ_{Simpl}	2.60 ± 0.01	2.56 ± 0.02	2.50 ± 0.02	2.55 ± 0.01	2.53 ± 0.02	2.50 ± 0.02	2.53 ± 0.01	2.60 ± 0.01
	f_{sc}	$0.232^{+0.010}_{-0.005}$	0.20 ± 0.01	0.20 ± 0.01	0.24 ± 0.01	$0.22^{+0.02}_{-0.01}$	0.22 ± 0.02	0.23 ± 0.01	0.23 ± 0.01
	$L^{(2)}_{Simpl}/L_{Edd}$	0.302 ± 0.004	0.184 ± 0.003	0.201 ± 0.003	0.241 ± 0.005	0.220 ± 0.004	0.126 ± 0.004	0.207 ± 0.004	0.277 ± 0.005
Nthcomp	$\Gamma_{Nthcomp}$	$1.89^{+0.06}_{-0.04}$	$1.88^{+0.08}_{-0.1}$	1.96 ± 0.08	$1.71^{+0.11}_{-0.13}$	$1.91^{+0.11}_{-0.15}$	$1.59^{+0.17}_{-0.19}$	$1.55^{+0.13}_{-0.15}$	$1.88^{+0.08}_{-0.11}$
	kT_e (eV)	$158.07^{+4.04}_{-4.25}$	$160.77^{+5.41}_{-5.40}$	$164.07^{+5.80}_{-5.32}$	$151.15^{+5.27}_{-5.21}$	$155.81^{+6.41}_{-7.49}$	$150.31^{+8.01}_{-7.19}$	$143.50^{+5.02}_{-4.70}$	$155.69^{+4.80}_{-5.55}$
	kT_{bb} (eV)	< 30.03	< 29.81	< 188.56	$33.12^{+1.91}_{-2.52}$	$32.46^{+2.03}_{-2.26}$	$33.08^{+1.86}_{-2.55}$	$34.97^{+1.58}_{-1.93}$	< 31.91
	$L^{(3)}_{Nthcomp}/L_{Edd}$	$0.284^{+0.005}_{-0.006}$	$0.195^{+0.004}_{-0.005}$	0.186 ± 0.005	0.236 ± 0.004	0.200 ± 0.004	0.135 ± 0.003	0.216 ± 0.004	0.261 ± 0.005
zgauss	E_{Line} (keV)	$6.80^{+0.25}_{-0.24}$	6.61 ± 0.15	$6.69^{+0.20}_{-0.21}$	$6.77^{+0.15}_{-0.14}$	$6.66^{+0.19}_{-0.18}$	6.67 ± 0.16	6.55 ± 0.13	$6.41^{+0.22}_{-0.23}$
	$F^{(4)}_{Line}$ (10^{-5})	$2.58^{+0.66}_{-0.68}$	2.90 ± 0.62	2.69 ± 0.71	$3.33^{+0.63}_{-0.62}$	$2.88^{+0.68}_{-0.66}$	2.7 ± 0.6	3.36 ± 0.62	$2.86^{+0.71}_{-0.69}$
χ^2/dof		307.78/251	375.10/248	358.36/247	357.22/250	324.17/248	277.84/238	359.74/249	349.05/248
χ^2_ν		1.24	1.51	1.45	1.43	1.31	1.17	1.44	1.41

(1) Maximum optical depth for absorption at the threshold energy.
(2) Normalized hard X-ray luminosity.
(3) Normalized soft X-ray luminosity.
(4) Line flux or the normalization of the redshifted gaussian line in units of photons cm^{-2} s^{-1}

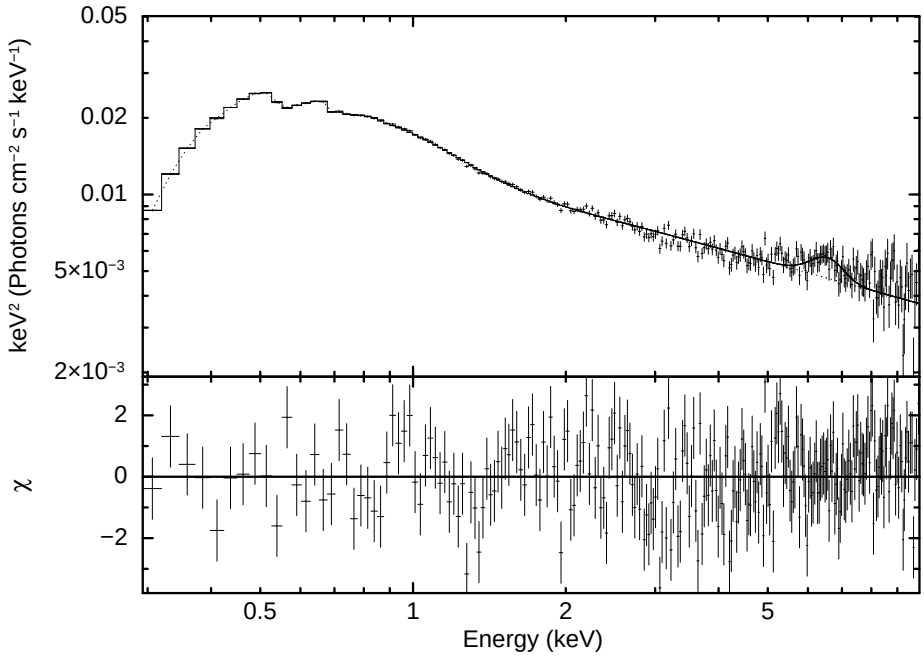

Figure 3 Top panel: The Unfolded EPIC-pn spectral data and the best-fitting model *zedge*×*zedge*×*TBabs*(*Simpl*⊗*Nthcomp*+*zgauss*) for Observation Number 2. Bottom panel: The deviation of the observed data from the model.

Extrapolation of the model down to 0.3 keV provided a poor fit indicating the presence of soft excess in the spectrum. We attempted to describe this soft excess with the thermal Comptonization XSPEC model *Nthcomp*. In this model, the temperature kT_{bb} of seed photons from the accretion disc (blackbody or disc blackbody) parameterizes the low energy cut-off, while the high energy roll over is given by the electron temperature kT_e ($\sim$ 160 eV). We assume that the photons from this component are the seed photons to the second thermal component giving rise to the high energy power law emission. Hence, we re-analysed the data replacing the *powerlaw* by introducing the convolution XSPEC model (*Simpl*) which transfers a fraction of the seed photons in the input spectrum into a power law (Steiner et al., 2009). The model yielded an unacceptable fit statistic of χ^2/dof=547.48/253. Inspection of the residuals revealed that the soft part of the spectrum was affected by an absorption feature around 0.7 keV. A better $\chi^2 = 385.74$ for 251 dof was obtained for the same observation, when we fitted the region with a redshifted absorption edge model, *zedge*. Another absorption feature was also found at $\sim$0.5 keV and it was modelled using one more *zedge*. Correspondingly the χ^2 was improved by $\Delta\chi^2 = -9.92$ which clearly shows the significance of including the new absorption feature. We also tried to model these features using more complex models such as *zxipcf* and *grid22soft* and obtained fit statistics comparable to the phenomenological two edge model. Moreover, the relevant spectral parameters such as the hard and soft X-ray fluxes and high energy spectral index are not sensitive to the absorption model used. Thus we proceed with the simple phenomenological model of two edges in this work. For this model, we show the unfolded spectrum and residuals in Fig. 3.

In order to study the relationship between X-ray and UV emission, we need to fit the spectra simultaneously. For this we loaded the *UVW2* data along with the pn data and then added the model *ezdiskbb* which describes the accretion disc spectrum consisting of multiple blackbody components (Zimmerman et al., 2005). The model is defined by two parameters, the inner disc temperature kT_{in}

and the norm N_{disk}, where N_{disk} is determined by the inner disc radius and the inclination of the disc. Further the effect of interstellar extinction on the source spectrum was taken into account using the model *uvred*, based on Seaton's law (Seaton, 1979). This UV reddening model is valid only in the range $1000-3074$ Å, and can be used in combination with photoelectric absorption models. The parameter E(B-V) was determined from the reddening law $R_V = A_V$/E(B-V) (Fitzpatrick, 1999) and the A_V magnitude of 0.198 was obtained from original SFD98 values assuming $R_V = 3.1$. So the value of E(B-V) was fixed to 0.064 for all observations. Then we fitted the *UVW2* data simultaneously with the EPIC-pn data by tying the parameter kT_{in} to the kT_{bb} of *Nthcomp*. This left only the normalisation of the *ezdiskbb* model as a free parameter to fit the single UV data point. To ensure that only the outer disc emission is used to fit the UV data point, we fixed the normalisation of the Comptonization component at a negligible value for the UV part of the spectrum. The best fit parameters for this model for all the observations are given in Table 3.

We have also calculated the X-ray flux for each model component in the range $0.3-10$ keV using the XSPEC convolution model *cflux*. The flux corresponding to the model component *Simpl* was calculated from the unabsorbed X-ray flux and the *Nthcomp* flux. It was obtained by subtracting $(1 - f_{sc})$ times the *Nthcomp* flux from the unabsorbed flux. Using the luminosity distance of *D*=98.5Mpc, by assuming the cosmological parameters H_0=73 km s^{-1} Mpc^{-1}, Ω_m=0.27 and Ω_Λ=0.73, we obtained the luminosities of each component.

The normalisation of the *ezdiskbb* model, N_{disc} is related to the inner disc radius R_{in} by

$$R_{in}(km) = f^2 \left(\frac{N_{disc}}{\cos i} \right)^{1/2} D_{10kpc}, \quad (1)$$

where D_{10kpc} is the luminosity distance to the source in units of 10 kpc. *i* is the inclination angle assumed here to be 30° and *f* stands for the colour correction factor which we assume to be the generally accepted value of 1.7. The mass accretion rate can be obtained using (Zimmerman et al., 2005)

$$\dot{M} = \frac{8\pi\sigma}{3GM} \left(\frac{T_*}{f} \right)^4 R_{in}^3, \quad (2)$$

where $T_* = T_{in}/0.488$. Several previous studies have estimated the black hole mass of Ark 564 to be in the range $(1.15 - 10)\times10^6 M_\odot$ (e.g. Pounds et al. (2001), Wang & Lu (2001), Bian & Zhao (2003), Botte et al. (2004), Zhou & Wang (2005), Zhang & Wang (2006)). In this study, we adopt the value 2.61×10^6 $M_\odot$ (Botte et al., 2004) obtained from stellar velocity dispersions. This allows us to express the luminosities in terms of the Eddington Luminosity L_{Edd} and the accretion rate in terms of the Eddington accretion rate, $\dot{M}_{Edd} = \frac{L_{Edd}}{\eta c^2}$, where η is the efficiency factor taken as 0.1. The normalised luminosities for the different observations are listed in Table 3.

5 UV & X-RAY CORRELATIONS

We investigate the correlation between varying X-ray spectral parameters, luminosities and F_{UV}. We identify the variable parameters by fitting a constant to the best-fit values obtained from different observations using χ^2 analysis. The reduced χ^2 values are listed in Table 4, with the larger reduced χ^2 values corresponding to highly variable parameters. Apart from the luminosities of the X-ray components and the UV flux, the high energy photon index Γ_{Simpl} is also found to be variable. Hence we restrict our correlation analysis to these parameters.

Since the nature of the relations between the parameters are unknown we need a non-parametric method to calculate the correlation. So we use Spearman's rank-order correlation (Press et al., 1992) to reveal any correlations. The rank and significance of correlations for different parameters are listed in Table 5. Fig. 4 and Fig. 5 show the plots of different parameters for which we find significant correlations.

In the X-ray domain, the soft excess luminosity $L_{Nthcomp}$ is well correlated to the high energy power law luminosity L_{Simpl}. In fact it seems that Γ_{simpl} is better correlated with $L_{Nthcomp}$ than it

Table 4 Reduced χ^2 values for constant model fits to spectral parameters derived from eight observations

Model	Parameter	χ^2_ν
zedge (at ∼0.7 keV)	E_{edge}	0.76
	τ_{max}	1.16
zedge (at ∼0.5 keV)	E_{edge}	2.69
	τ_{max}	1.18
ezdiskbb	N_{disc}	0.12
Simpl	Γ_{Simpl}	6.13
	f_{sc}	1.53
Nthcomp	$\Gamma_{Nthcomp}$	1.58
	kT_e	1.56
	kT_{bb}	0.23
	$N_{Nthcomp}$	26.07
zgauss	E_{Line}	0.42
	F_{Line}	0.21
Flux	F_{UV}	61.79
Luminosity	$L_{Nthcomp}$	129.15
	L_{Simpl}	200.41

Table 5 Spearman's correlation between different parameters. Column 3: Spearman's rank-order correlation coefficient. Column 4: p-value

Parameter 1	Parameter 2	r	p
F_{UV}	Count Rate $_{X-ray}$	0.69	0.06
F_{UV}	$L_{Nthcomp}/L_{Edd}$	0.71	0.05
F_{UV}	L_{Simpl}/L_{Edd}	0.57	0.14
F_{UV}	Γ_{Simpl}	0.93	0.0009
$L_{Nthcomp}/L_{Edd}$	L_{Simpl}/L_{Edd}	0.95	0.0003
$L_{Nthcomp}/L_{Edd}$	Γ_{Simpl}	0.78	0.02
L_{Simpl}/L_{Edd}	Γ_{Simpl}	0.69	0.06

is with the high energy luminosity L_{Simpl}, in the sense that the null hypothesis probability p is significantly smaller. As we discuss in the next section these correlations are consistent with the double Comptonization model used for the spectral fitting.

For the UV−X-ray correlations, we note that there is not much evidence for any correlation between F_{UV} and the X-ray luminosities in the two Comptonization component $L_{Nthcomp}$ and L_{Simpl} with probabilities of $p = 0.05$ and 0.14. However a strong correlation is seen for F_{UV} and Γ_{simpl} with $p = 0.0009$.

6 SUMMARY AND DISCUSSION

We have analysed the simultaneous X-ray (EPIC-pn) and UV (OM *UVW2*) data from eight *XMM-Newton* observations of Ark 564 taken in 2011. We used the thermal Comptonization models favoured by Dewangan et al. (2007) for the spectral fitting of the X-ray data. The soft X-ray spectrum (0.3−3 keV) was modelled by *Nthcomp* assuming that the UV photons emitted from the accretion disc are Comptonized by the optically thick corona leading to the soft excess emission. The accretion disc emitting the seed photons is described by the multicolour black body model *ezdiskbb*. Further, the hard X-ray power law emission (3−10 keV) is taken into account by the second Comptonization model *Simpl* which incorporates the physics of Compton upscattering of soft photons by hot coronal electrons. We report that this double Comptonization model fits all the eight spectra well.

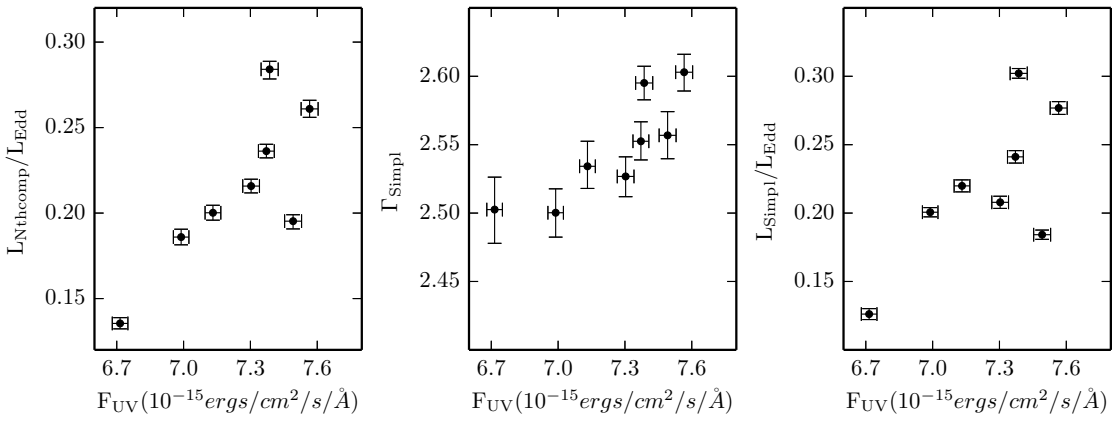

Figure 4 The variation of different parameters with UV flux F_{UV}. The left and right panels respectively show the soft and the hard X-ray luminosities as a function of F_{UV}. The middle panel depicts the dependence of Γ_{Simpl} on F_{UV}. The luminosities are expressed relative to the Eddington value.

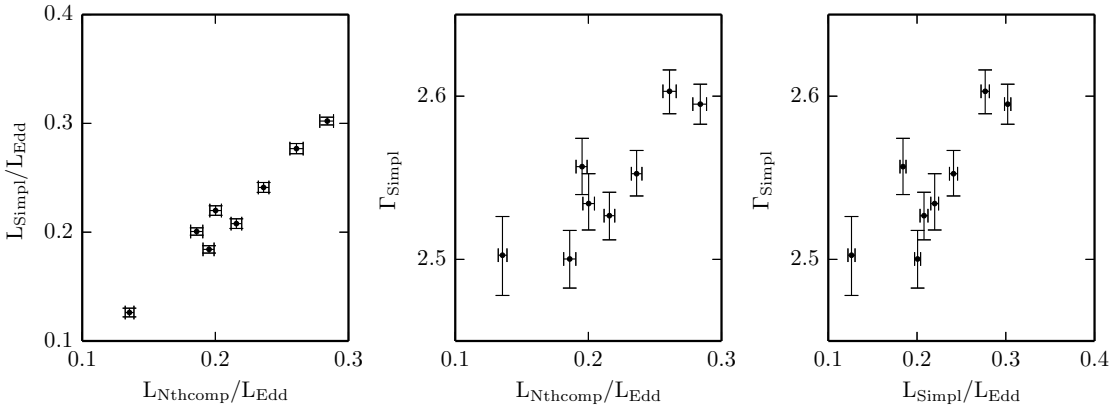

Figure 5 The correlation of different parameters. The luminosities are denoted in units of Eddington luminosity. Left & Middle panels: The variation of hard X-ray luminosity and hard X-ray photon index with soft X-ray luminosity. Right Panel: The dependence of hard X-ray photon index on the hard X-ray luminosity.

In the X-ray band, we find that the luminosity of the soft Comptonization component $L_{nthcomp}$ correlates well with the hard component L_{Simpl}. While there is some evidence that the high energy index Γ_{Simpl} correlates well with both luminosities, there is a seemingly stronger correlation between Γ_{Simpl} and $L_{nthcomp}$ in the sense that null hypothesis probability is smaller. There have been several studies which have shown that the high energy index is correlated with the X-ray flux (e.g.Dewangan (2002), Vaughan & Edelson (2001), Perola et al. (1986)). Recently, Sarma et al. 2015 have studied the index versus flux variation for Mrk 335 and Ark 564 and have reported that while the correlation exists for both sources, there is significantly more scatter for Ark 564. Our results are broadly consistent with

their finding and perhaps gives an explanation for the difference between the two sources. Also the correlations obtained here are consistent with the double Comptonization model used.

There is little evidence for any correlation between the UV flux and the hard component luminosity with null hypothesis probability of $p = 0.14$. There is a hint of a correlation between the UV flux and the soft X-ray component luminosity with $p = 0.05$. However, the UV flux is strongly correlated to the photon index Γ_{Simpl}.

We can interpret the correlation between UV and X-ray emissions in two different ways. One interpretation is that the variation in UV emission could be due to the accretion rate fluctuation. So as the UV flux varies, it provides a way to measure the accretion rate $\dot{m}$ as a fraction of the Eddington rate and it is found to vary from $\sim$3.7 to $\sim$4.4. However, one can estimate from the accretion rate that the measured UV emission should mostly arise from the outer disc at a distance of $\sim 770R_g$, where R_g is the Schwarzschild radius. At this radius the viscous time-scale is $t_{visc} \sim 9$ years, which is much longer than the 6 day variability seen; more importantly, the variation in accretion rate could not have propagated to the inner regions in such short time-scales. We can further estimate that less than 2% of the UV flux would arise from radii $\sim 30R_g$. If the flux variation at those radii is very large, it may give rise to the $\sim$1% variation seen in the UV. However, even at $\sim 30R_g$ the viscous time-scale is too long at $\sim$ 61 days. Moreover, the accretion rate inferred from this interpretation is significantly higher than the Eddington rate and hence unlikely. Thus, it seems that the UV emission, or at least its variability cannot arise due to accretion rate fluctuations.

The second possibility is that the UV flux variation is due to the reprocessing of X-rays. In such a case our results indicate that the soft X-ray emitting region and Γ_{Simpl} are more important in determining the X-ray irradiation than the X-ray luminosity itself. We note that recently Pal et al. (2016) have studied the UV-X-ray correlation on much shorter 20 ksec time-scales and have come to a similar conclusion that the geometry of the inner X-ray producing region may be playing an important role in determining the UV emission.

Though we have not used the blurred reflection model (e.g., Fabian et al. 2002) to describe the soft X-ray excess and the broad iron line observed from Ark 564, the model can be tested against the observed correlations. In the blurred reflection model, the soft excess and the broad iron line are physically the same spectral component, and hence these two features must be strongly correlated. The presence of the broad iron line strongly suggests some contribution of the blurred reflection to the soft X-ray excess. Indeed, the observation of reverberation soft lags of $\sim 100\ s$ in Ark 564 by Kara et al. (2013) clearly demonstrate the presence of blurred reflection in the soft ($0.3-1$ keV) band. However, the findings of soft leads in Ark 564 (Dewangan, 2002; Kara et al., 2013) suggest contribution of additional spectral component in the soft band. In our analysis, the broad iron line does not appear to follow the strongly variable soft X-ray excess emission. Illumination of the hard X-ray power law component should not only result in the blurred reflection (the soft excess, broad iron line and the hump in the $\sim 20 - 40$ keV) but also in the reprocessed emission in the UV band. The correlation between F_{UV} and L_{Simpl} may result from the reprocessing of the coronal X-ray emission in the disc. However, the similar variability amplitudes of the soft excess and the hard X-ray emission is difficult to explain in the reflection model in which a compact corona along the symmetrical axis illuminates the disc. In such a model, due to the bending of light, the reflected emission that includes the soft excess and the iron line is much less variable than the illuminating power law (Miniutti & Fabian, 2004). Thus, the observed strong soft X-ray excess entirely is unlikely to be the reflected emission.

Our results are based on eight observations separated by $\sim$6 days and clearly there is a need for a larger number of such observations to verify these interpretations. Further long term simultaneous monitoring of UV and X-ray emissions over different time-scales can give us more insight into the variability of the source. Also the results can be compared with correlations obtained for other AGN. This may be possible with *ASTROSAT* which has the Ultra Violet Imaging Telescope (*UVIT*) for monitoring the UV emission and the Soft X-ray imaging Telescope (*SXT*) and the Large Area X-ray Proportional Counters (*LAXPC*) for X-ray studies.

ACKNOWLEDGMENTS

This study is based on the observations obtained with *XMM-Newton* satellite, an ESA science mission with instruments and contributions directly funded by ESA Member States and the USA (NASA). This work has made use of the NASA/IPAC Extragalactic Data base which is operated by the Jet Propulsion Laboratory, California Institute of technology and data obtained through the High Energy Astrophysics Science Archive Research Center Online Service, provided by the NASA/GSFC. The first author would like to thank the Department of Science and Technology for the support grant (No.SR/S2/HEP-07/2012) for this work.

References

Beckmann, V., & Shrader, C. 2012, AGN Types and Unification, Active Galactic Nuclei (Wiley-VCH Verlag GmbH and Co. KGaA), 89
Bian, W., & Zhao, Y. 2003, MNRAS, 343, 164
Boller, T., Brandt, W. N., & Fink, H. 1996, A&A, 305, 53
Botte, V., Ciroi, S., Rafanelli, P., & Di Mille, F. 2004, AJ, 127, 3168
Brandt, W. N., Fabian, A. C., Nandra, K., Reynolds, C. S., & Brinkmann, W. 1994, MNRAS, 271, 958
Brinkmann, W., Papadakis, I. E., & Raeth, C. 2007, A&A, 465, 107
Dewangan, G. C. 2002, ApJ, 581, L71
Dewangan, G. C., Griffiths, R. E., Dasgupta, S., & Rao, A. R. 2007, ApJ, 671, 1284
Edelson, R. A., Alexander, T., Crenshaw, D. M., et al. 1996, ApJ, 470, 364
Fabian, A. C., Ballantyne, D. R., Merloni, A., et al. 2002, MNRAS, 331, L35
Fitzpatrick, E. L. 1999, PASP, 111, 63
Giustini, M., Turner, T. J., Reeves, J. N., et al. 2015, arXiv:1502.01338
Kalberla, P. M. W., Burton, W. B., Hartmann, D., et al. 2005, A&A, 440, 775
Kara, E., Fabian, A. C., Cackett, E. M., et al. 2013, MNRAS, 434, 1129
Legg, E., Miller, L., Turner, T. J., et al. 2012, ApJ, 760, 73
Matsumoto, C., Leighly, K. M., & Marshall, H. L. 2004, ApJ, 603, 456
McHardy, I. M., Cameron, D. T., Dwelly, T., et al. 2014, MNRAS, 444, 1469
Miniutti, G., & Fabian, A. C. 2004, MNRAS, 349, 1435
Mullaney, J. R., Ward, M. J., Done, C., Ferland, G. J., & Schurch, N. 2009, MNRAS, 394, L16
Nandra, K., Clavel, J., Edelson, R. A., et al. 1998, ApJ, 505, 594
Pal, M., Dewangan, G. C., Misra, R., & Pawar, P. K. 2016, MNRAS, 457, 875
Perola, G. C., Piro, L., Altamore, A., et al. 1986, ApJ, 306, 508
Peterson, B. M. 1997, An Introduction to Active Galactic Nuclei (Cambridge University Press), cambridge Books Online
Pounds, K., Edelson, R., Markowitz, A., & Vaughan, S. 2001, ApJ, 550, L15
Press, W. H., Teukolsky, S. A., Vetterling, W. T., & Flannery, B. P. 1992, Numerical recipes in FORTRAN. The art of scientific computing
Sarma, R., Tripathi, S., Misra, R., et al. 2015, MNRAS, 448, 1541
Seaton, M. J. 1979, MNRAS, 187, 73P
Shemmer, O., Uttley, P., Netzer, H., & McHardy, I. M. 2003, MNRAS, 343, 1341
Shemmer, O., Romano, P., Bertram, R., et al. 2001, ApJ, 561, 162
Smith, R., & Vaughan, S. 2007, MNRAS, 375, 1479
Steiner, J. F., McClintock, J. E., Remillard, R. A., Narayan, R., & Gou, L. 2009, ApJ, 701, L83
Strüder, L., Briel, U., Dennerl, K., et al. 2001, A&A, 365, L18
Turner, M. J. L., Abbey, A., Arnaud, M., et al. 2001, A&A, 365, L27
Vaughan, S., & Edelson, R. 2001, ApJ, 548, 694
Vaughan, S., Pounds, K. A., Reeves, J., Warwick, R., & Edelson, R. 1999, MNRAS, 308, L34
Vignali, C., Brandt, W. N., Boller, T., Fabian, A. C., & Vaughan, S. 2004, MNRAS, 347, 854
Wang, T., & Lu, Y. 2001, A&A, 377, 52

Wilms, J., Allen, A., & McCray, R. 2000, ApJ, 542, 914
Zhang, E.-P., & Wang, J.-M. 2006, ApJ, 653, 137
Zhou, X.-L., & Wang, J.-M. 2005, ApJ, 618, L83
Zimmerman, E. R., Narayan, R., McClintock, J. E., & Miller, J. M. 2005, ApJ, 618, 832